Journal of Medicinal Chemistry

Article

pubs.acs.org/jmc

# Chemical Probes to Study ADP-Ribosylation: Synthesis and Biochemical Evaluation of Inhibitors of the Human ADP-Ribosyltransferase ARTD3/PARP3

Anders E. G. Lindgren,[†] Tobias Karlberg,[‡] Torun Ekblad,[‡] Sara Spjut,[†] Ann-Gerd Thorsell,[‡] C. David Andersson,[†] Ton Tong Nhan,[†] Victor Hellsten,[†] Johan Weigelt,[‡] Anna Linusson,[†] Herwig Schüler,[‡] and Mikael Elofsson*[,†]

[†]Department of Chemistry, Umeå University, SE-90187 Umeå, Sweden

[‡]Department of Medicinal Biochemistry and Biophysics, Karolinska Institutet, SE-17177 Stockholm, Sweden

Supporting Information

**ABSTRACT:** The racemic 3-(4-oxo-3,4-dihydroquinazolin-2-yl)-*N*-[1-(pyridin-2-yl)ethyl]propanamide, **1**, has previously been identified as a potent but unselective inhibitor of diphtheria toxin-like ADP-ribosyltransferase 3 (ARTD3). Herein we describe synthesis and evaluation of 55 compounds in this class. It was found that the stereochemistry is of great importance for both selectivity and potency and that substituents on the phenyl ring resulted in poor solubility. Certain variations at the meso position were tolerated and caused a large shift in the binding pose. Changes to the ethylene linker that connects the quinazolinone to the amide were also investigated but proved detrimental to binding. By combination of synthetic organic chemistry and structure-based design, two selective inhibitors of ARTD3 were discovered.

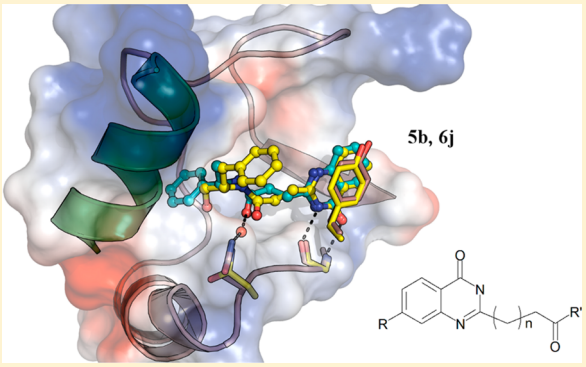


## 1. INTRODUCTION

The human diphtheria toxin-like ADP-ribosyltransferase (ARTD) family consists of 17 different proteins that all share a conserved catalytic domain.[1,2] These enzymes use nicotinamide adenine dinucleotide ($NAD^+$) as a donor of ADP-ribose units. The ARTD family can be further divided into two major subgroups. The mono-ADP-ribose transferases (mARTs) transfer single ADP-ribose moieties onto their targets, while the poly-ADP-ribose polymerases (PARPs) catalyze the transfer of ADP-ribose moieties onto growing chains of ADP-ribose on their target proteins.[3] In recognition of this, we chose to adopt the nomenclature proposed by Hottiger et al.[1] for the family of proteins previously known as PARPs.

Although protein ADP-ribosylation was discovered more than 40 years ago, its biological relevance is still poorly understood, and most of the enzymes that catalyze ADP-ribosylation are not well characterized.[4] ADP-ribosylation plays critical roles in several cellular processes, including cell differentiation, proliferation, and maintenance of genome integrity.[5,6] The two most abundant ARTDs in human are ARTD1/PARP1 and its closest relative ARTD2/PARP2. ARTD1, which is involved in chromatin remodeling, DNA repair, and apoptosis,[7] has been of interest in drug discovery for over a decade, and ARTD inhibitors are currently undergoing clinical studies for treatment of several forms of cancer.[8,9]

Currently known ARTD inhibitors are promiscuous within the protein family, and studying individual ARTDs *in vivo* is difficult.[1,10] Selective inhibitors would be invaluable tools to improve our understanding of the medically important ARTD proteins. We set out to develop small molecules, dubbed chemical probes, for use as research tools to study ADP-ribosylation and its role in cellular systems by selectively inhibiting single family members.

Previously, a focused library consisting of 185 compounds, many of them $NAD^+$ mimics, was tested against 13 members of the human ARTD family in a thermal shift assay.[10] Together with crystal structures of ARTD catalytic domain−ligand complexes, this served as a powerful tool for elucidating how the structure of a novel compound affected the binding mode, activity and selectivity and allowed a considerably more efficient structure-based approach.

Herein we describe the design, synthesis and evaluation of 44 novel and 11 commercial compounds and their potency and selectivity with respect to inhibition of ARTD3/PARP3 and ARTD1/PARP1.

## 2. RESULTS AND DISCUSSION

Evaluation of the binding of 185 compounds to 13 ARTD enzyme catalytic domains indicated that **1** (Table 1) was a suitable starting point for a medicinal chemistry program. The rationale for this choice was the apparently tight binding and

**Received:** July 5, 2013
**Published:** November 4, 2013

**Table 1. Selectivity Data for 1, an ARTD3 Binder Identified by Use of a Thermal Stabilization Assay[a]**

| Entry | ID | Structure | ARTD3 $\Delta T_m$ (°C) | ARTD1 $\Delta T_m$ (°C) | ARTD2 $\Delta T_m$ (°C) | ARTD5 $\Delta T_m$ (°C) | ARTD8 $\Delta T_m$ (°C) |
|---|---|---|---|---|---|---|---|
| 1[a] | **1** | 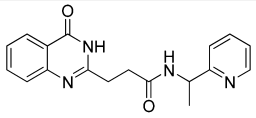 | 8.46 ± 0.17 | 1.98 ± 0.06 | 1.35 ± 0.43 | 0.00 ± 0.04 | -0.29 ± 0.51 |

[a]Data were previously published.[12] ARTD3 shares a higher degree of similarity with ARTD1 and ARTD2 than with ARTD5/tankyrase-1 and ARTD8/PARP14.[2,11]

**Scheme 1. Synthesis of 5a−f, 6a−m, 7a−f, 18a−f, and 19b−h**

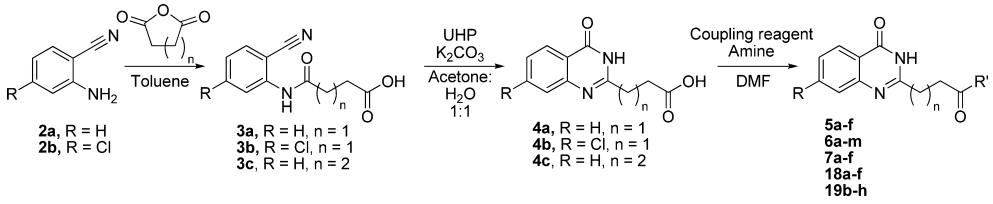


**Table 2. Thermal Shift Data for 5a−i against Five Members of the ARTD Family[a]**

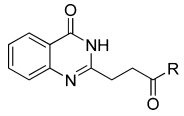

| Entry | ID | R | ARTD3 $\Delta T_m$ (°C) | ARTD1 $\Delta T_m$ (°C) | ARTD2 $\Delta T_m$ (°C) | ARTD5 $\Delta T_m$ (°C) | ARTD8 $\Delta T_m$ (°C) |
|---|---|---|---|---|---|---|---|
| 1[a] | **5a** | 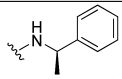 | 5.97 ± 0.47 | 3.05 ± 0.03 | 1.95 ± 0.18 | 0.35 ± 0.02 | -0.22 ± 0.12 |
| 2[a] | **5b** | 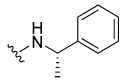 | 8.45 ± 0.59 | 1.80 ± 0.05 | 1.16 ± 0.10 | 0.13 ± 0.05 | -0.23 ± 0.08 |
| 3[a] | **5c** | 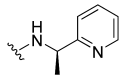 | 4.79 ± 0.21 | 2.35 ± 0.08 | 1.26 ± 0.25 | 0.12 ± 0.05 | -0.23 ± 0.06 |
| 4[a] | **5d** | 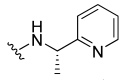 | 9.71 ± 0.39 | 1.96 ± 0.24 | 0.74 ± 0.55 | 0.13 ± 0.06 | 0.31 ± 0.25 |
| 5 | **5e** | 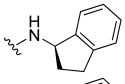 | 6.84 ± 0.14 | 2.37 ± 0.01 | 1.92 ± 0.27 | 0.80 ± 0.07 | 0.10 ± 0.28 |
| 6 | **5f** | 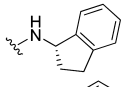 | 6.72 ± 0.49 | 2.38 ± 0.05 | 1.39 ± 0.08 | 0.84 ± 0.07 | 0.18 ± 0.09 |
| 7[b] | **5g** | 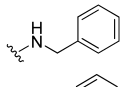 | 2.63 ± 0.30 | 2.16 ± 0.03 | 1.77 ± 0.22 | 0.32 ± 0.06 | -0.28 ± 0.19 |
| 8[b] | **5h** | 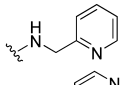 | 4.83 ± 0.26 | 1.93 ± 0.02 | 1.48 ± 0.15 | 0.15 ± 0.08 | -0.25 ± 0.04 |
| 9[b,c] | **5i** | 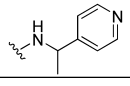 | 5.02 ± 0.52 | 2.68 ± 0.01 | 1.82 ± 0.59 | 0.30 ± 0.05 | 0.00 ± 0.12 |

[a]Data previously published.[12] [b]Commercial compounds not synthesized as a part of this work. [c]Racemic mixture.

selectivity suggested by the $T_m$-shift data (Table 1), paired with straightforward synthesis of analogues that allowed a large degree of diversity to be introduced in the last reaction step (Scheme 1). The low molecular weight and low lipophilicity of **1** were also advantageous, as these properties tend to increase as compounds are being further optimized.

**2.1. Stereochemistry and Heteroatoms.** Compound **1** was tested as a racemate. Thus, it was crucial to determine the importance of the stereochemistry of the methyl group, and the two enantiomers of **1** were synthesized separately according to Scheme 1. The importance of the nitrogen in the pyridinyl moiety was also investigated at an early stage, since a large number of different benzylamines are readily available while their pyridinyl analogues are scarce.[13] Finally, two cyclized analogues were synthesized in order to explore the effect of a more rigid structure (Table 2).

A general synthetic route to compounds **5a−f** is presented in Scheme 1. Reacting 2-aminobenzonitrile, **2a**, with succinic


dx.doi.org/10.1021/jm401394u | J. Med. Chem. 2013, 56, 9556−9568

anhydride in toluene gave the resulting anilide, **3a**, in 96% yield. Compound **3a** was then ring-closed to the quinazolinone main fragment **4a** in 68% yield by use of urea hydrogen peroxide (UHP) and potassium carbonate.[14] Finally, **5a−f** were obtained from **4a** in 53−78% yield by use of *N*,*N*′-diisopropylcarbodiimide (DIC) and 1-hydroxybenzotriazole (HOAt)[15] together with the appropriate amines. The amines corresponding to **5c** and **5d**, (*R*)- and (*S*)-1-(pyridin-2-yl)ethanamine, were not commercially available but were instead synthesized from their respective alcohols by use of diphenyl phosphoryl azide (DPPA) to produce the azides, which were then reduced to the amines under Staudinger reduction conditions.[16]

The recently synthesized **5a−f** and the library substances **5g−i** were evaluated by thermal shift assay. In brief, protein solutions in phosphate-buffered saline (PBS) with tris(2-carboxyethyl)phosphine (TCEP) and SyproOrange were added to wells containing compound solution. Thermal stability was then measured by monitoring SyproOrange fluorescence while heating the samples, and determining the midpoints of the transitions. Previous investigations showed that this assay gives a good estimate of binding affinity, adequate to indicate the direction in which a medicinal chemistry program should be focused.[10]

As shown in Table 2, the enantiomers with *S* as absolute configuration at the meso position (**5b** and **5d**) produced considerably higher $\Delta T_m$ values and showed better selectivity toward ARTD3 compared to the *R* enantiomers (**5a** and **5c**). Importantly, removing the pyridinyl ring in favor of an unsubstituted phenyl ring did not lead to any significant drop in either affinity or selectivity. Rigidifying the structure, as in **5e** and **5f**, diminished the importance of the stereochemistry and decreased selectivity toward ARTD3. Also, a substituent at the meso position (**5g** and **5h**) was necessary in order to maintain affinity and selectivity. Finally, the poor effect of the racemate **5i** indicated that shifting the nitrogen to the para position was unfavorable. The crystal structure of the complex of ARTD3 and **5i** can provide an explanation; this nitrogen is involved in water-mediated hydrogen bonds with the carbonyl group of Asp291, shifting the position of the ring about 1 Å outward from the pocket compared to **5b**, resulting in a poorer fit (Figure 1a).

**2.2. Substitution Patterns.** On the basis of results from the previous compounds in combination with the recently determined crystal structures of ARTD3 with **5b** and **5d**[12] (Figure 1b), it was decided that the ensuing work should be focused on phenyl rings instead of their pyridinyl counterparts. As shown in Figure 1, the bifurcated interaction between the amide part of the quinazolinone and Gly385 in the backbone of ARTD3 anchors the ligand inside the nicotinamide pocket. This interaction is the hallmark of ARTD inhibitors based on nicotinamide mimetics. In addition to these interactions, **5a** and **5b** form a water-mediated hydrogen bond between the amide group carbonyl oxygen and the Asn387 side chain. The amide group of the *R* enantiomer **5c** (thus also **5a**) is instead rotated away from Asn387, resulting in a missing hydrogen-bonding opportunity with an associated loss of affinity (Figure 1c). Additionally, crystal structures show that the pyridinyl nitrogen in **5d** does not find any favorable interactions with ARTD3 and is thus considered nonessential. However, the nitrogen does produce favorable interactions with ARTD1 that slightly lower the ARTD3 selectivity of this compound.[12]

A new series of compounds (Table 3, **6a−m**) was designed and synthesized via the above procedure (Scheme 1) in order to further explore the importance of stereochemistry and functionalization at the meso position. Compounds **6a−d** probed

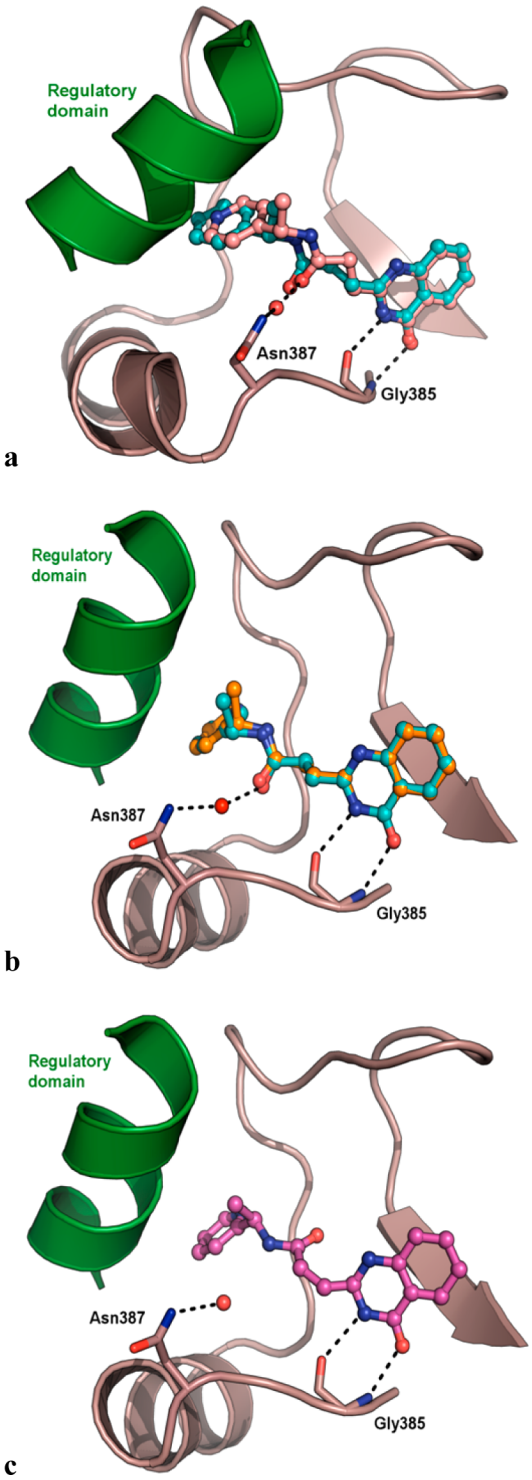


**Figure 1.** Binding of inhibitors to the cosubstrate $NAD^+$ binding site of ARTD3. Consensus helix αF of the regulatory domain, which makes up one side of the distal end of the $NAD^+$ binding pocket, is shown in green. (a) Compounds **5b** (teal, PDB ID 4GV4) and **5i** (salmon, PDB ID 4L6Z) in ARTD3. The ring structure in **5i** has moved about 1 Å outward from the pocket compared to **5b**. (b) Compounds **5b** (teal, PDB ID 4GV4) and **5d** (orange, PDB ID 4GV0) in ARTD3. The conformation of the protein is highly conserved and the binding poses of the ligands are similar. (c) Compound **5c** in ARTD3 (PDB ID 4GV2). The amide carbonyl is rotated away from Asn387.


dx.doi.org/10.1021/jm401394u | *J. Med. Chem.* 2013, 56, 9556−9568

Table 3. Thermal Shift Data for 6a−r against Five Members of the ARTD Family[a]

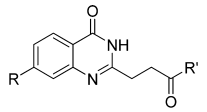

| Entry | ID | R | R' | ARTD3 $\Delta T_m$(°C) | ARTD1 $\Delta T_m$(°C) | ARTD2 $\Delta T_m$(°C) | ARTD5 $\Delta T_m$(°C) | ARTD8 $\Delta T_m$(°C) |
|---|---|---|---|---|---|---|---|---|
| 1 | **6a** | H | 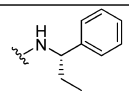 | 2.80 ± 0.15 | 1.49 ± 0.02 | 0.94 ± 0.14 | 0.33 ± 0.06 | 0.31 ± 0.08 |
| 2[b] | **6b** | H | 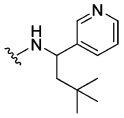 | 5.96 ± 0.36 | 0.9 ± 0.03 | 0.74 ± 0.16 | 0.44 ± 0.04 | 0.16 ± 0.10 |
| 3 | **6c** | H | 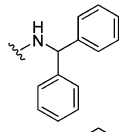 | 0.20 ± 0.04 | 0.2 ± 0.06 | 0.30 ± 0.27 | 0.22 ± 0.02 | 0.45 ± 0.54 |
| 4 | **6d** | H | 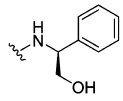 | 3.57 ± 0.31 | 2.83 ± 0.07 | 1.64 ± 0.12 | 0.82 ± 0.13 | 0.38 ± 0.42 |
| 5 | **6e** | H | 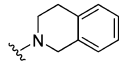 | 4.73 ± 0.14 | 1.15 ± 0.16 | -0.17 ± 0.18 | 0.14 ± 0.11 | -0.07 ± 0.01 |
| 6 | **6f** | H | 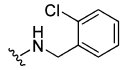 | 5.39 ± 0.40 | 1.85 ± 0.12 | 1.64 ± 0.14 | 0.48 ± 0.03 | 0.26 ± 0.13 |
| 7 | **6g** | H | 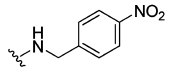 | 3.29 ± 0.42 | 4.00 ± 0.16 | 0.53 ± 0.39 | 0.97 ± 0.05 | -0.11 ± 0.21 |
| 8 | **6h** | H | 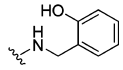 | 6.31 ± 0.64 | 2.79 ± 0.11 | 1.30 ± 0.35 | 0.70 ± 0.06 | -0.27 ± 0.04 |
| 9 | **6i** | H | 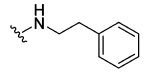 | 6.23 ± 0.27 | 2.83 ± 0.05 | 1.57 ± 0.19 | 0.49 ± 0.02 | 0.20 ± 0.39 |
| 10 | **6j** | H | 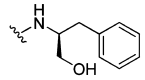 | 9.82 ± 0.39 | 3.59 ± 0.02 | 1.37 ± 0.17 | 0.60 ± 0.05 | 0.08 ± 0.16 |
| 11 | **6k** | Cl | 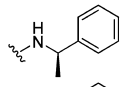 | 0.16 ± 0.05 | 0.92 ± 0.23 | 1.28 ± 0.21 | 0.43 ± 0.04 | 0.05 ± 0.34 |
| 12 | **6l** | Cl | 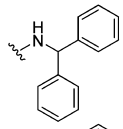 | 0.35 ± 0.10 | 0.11 ± 0.06 | 0.83 ± 0.18 | 0.20 ± 0.17 | 0.82 ± 0.05 |
| 13 | **6m** | Cl | 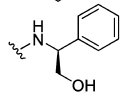 | 0.50 ± 0.06 | 0.76 ± 0.08 | 0.98 ± 0.03 | 0.36 ±0.04 | -0.25 ± 0.13 |
| 14[a] | **6n** | H | 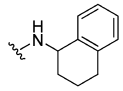 | 2.28 ± 0.47 | 2.44 ± 0.06 | 1.11 ± 0.21 | 1.83 ± 0.03 | 0.24 ± 0.05 |
| 15[a] | **6o** | H | 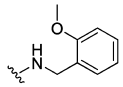 | 2.96 ± 0.34 | 1.45 ± 0.06 | 1.14 ± 0.21 | 0.54 ± 0.10 | 0.23 ± 0.29 |
| 16[a,b] | **6p** | H | 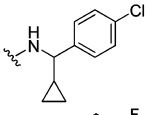 | 0.45 ± 0.07 | 2.17 ± 0.10 | 0.77 ± 0.22 | 0.52 ± 0.01 | -0.28 ± 0.88 |
| 17[a] | **6q** | H | 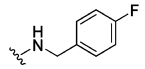 | 4.20 ± 0.12 | 3.11 ± 0.07 | 1.37 ± 0.24 | 0.69 ± 0.13 | 0.69 ± 0.18 |
| 18[a] | **6r** | H | 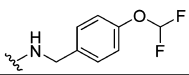 | 0.78 ± 0.23 | 3.39 ± 0.04 | 1.35 ± 0.19 | 0.96 ± 0.02 | 0.31 ± 0.62 |

[a]Commercial compounds. [b]Racemic mixture.



dx.doi.org/10.1021/jm401394u | J. Med. Chem. 2013, 56, 9556−9568

Table 4. Thermal Shift Data for 7a–k against Five Members of the ARTD Family

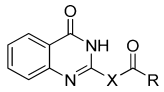

| Entry | ID | X | R | ARTD3 $\Delta T_m$(°C) | ARTD1 $\Delta T_m$(°C) | ARTD2 $\Delta T_m$(°C) | ARTD5 $\Delta T_m$(°C) | ARTD8 $\Delta T_m$(°C) |
|---|---|---|---|---|---|---|---|---|
| 1 | **7a** | $CH_2CH_2CH_2$ | 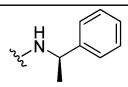 | 4.27 ± 0.15 | 1.56 ± 0.04 | 0.21 ± 0.25 | 1.37 ± 0.02 | -0.05 ± 0.19 |
| 2 | **7b** | $CH_2CH_2CH_2$ | 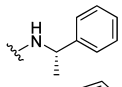 | 4.58 ± 0.25 | 1.51 ± 0.06 | 0.37 ± 0.32 | 0.52 ± 0.10 | -0.21 ± 0.14 |
| 3 | **7c** | $CH_2CH_2CH_2$ | 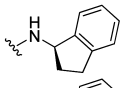 | 3.46 ± 0.06 | 1.52 ± 0.14 | 2.29 ± 0.16 | 1.20 ± 0.03 | 0.13 ± 0.24 |
| 4 | **7d** | $CH_2CH_2CH_2$ | 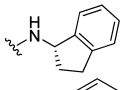 | 4.69 ± 0.18 | 1.88 ± 0.24 | 1.27 ± 0.33 | 0.59 ± 0.05 | -0.18 ± 0.17 |
| 5 | **7e** | $CH_2CH_2CH_2$ | 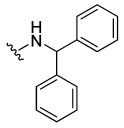 | 0.09 ± 0.06 | 0.44 ± 0.19 | 0.53 ± 0.17 | 0.41 ± 0.05 | 0.02 ± 0.26 |
| 6 | **7f** | $CH_2CH_2CH_2$ | 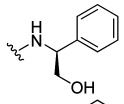 | 3.22 ± 0.17 | 2.90 ± 0.05 | 1.84 ± 0.08 | 1.05 ± 0.04 | 0.53 ± 0.17 |
| 7 | **7g** | (E)-CHCH | 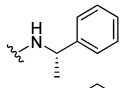 | 0.22 ± 0.06 | 1.22 ± 0.01 | -0.67 ± 0.08 | 0.42 ± 0.06 | -0.07 ± 0.13 |
| 8 | **7h** | $CH_2$ | 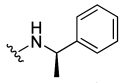 | 0.63 ± 0.16 | 0.37 ± 0.12 | -0.25 ± 0.09 | 0.05 ± 0.02 | -0.04 ± 0.13 |
| 9 | **7i** | $CH_2$ | 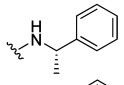 | 0.43 ± 0.02 | 0.31 ± 0.07 | -0.01 ± 0.21 | 0.01 ± 0.02 | 0.04 ± 0.09 |
| 10 | **7j** | $CH_2NH$ | 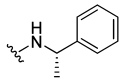 | 4.95 ± 0.45 | 0.88 ± 0.01 | 0.33 ± 0.29 | 0.39 ± 0.04 | -0.77 ± 0.25 |
| 11 | **7k** | $CH_2NH$ | 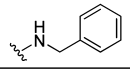 | 2.91 ± 0.05 | 0.65 ± 0.22 | -0.23 ± 0.18 | 0.34 ± 0.11 | -1.05 ± 0.73 |

Scheme 2. Synthesis of 7g

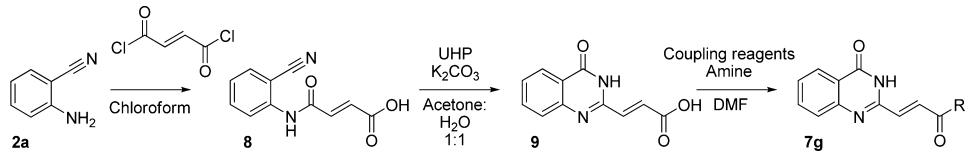


the possibilities of replacing the methyl group with larger substituents, while **6e** investigated how rigidifying **5g** would affect the mode of binding. Compounds **6f–j** were used to further study whether or not a substituent was needed at the meso position and how homobenzylic amides would influence the affinity. Finally, **6k–m**, with a chlorine substituent in the C7 position of the quinazolinone scaffold, were prepared to analyze whether lipophilic functional groups were allowed in this part of the binding pocket. Reaction conditions (Scheme 1) were modified accordingly to prepare the chloro-substituted ligands; the appropriate chloro-substituted aniline, **2b**, reacted with succinic anhydride to give **3b** in 64% yield, followed by alkali-mediated cyclization to give **4b** in 75% yield. Due to purification issues, *O*-(7-azabenzotriazol-1-yl)-*N*,*N*,*N*′,*N*′-tetramethyluronium hexafluorophosphate (HATU)[15] replaced DIC/HOAt in some of the amide couplings, which gave yields of 3–96% for this series of compounds. The reactions generally showed quantitative conversion, and no byproducts derivable from **4b** were observed regardless of the coupling reagents used. Thus, the low yields can be attributed to the difficulty of purifying some of these compounds.

Most of the modifications made to these compounds (Table 3) resulted in a decrease in thermal shift compared to **5b** and **5d**. One definite exception was **6j**, which, at the expense of decreased selectivity, showed the same affinity toward ARTD3 as the two previously top-ranked compounds. These results also indicated that the chlorine substituent was undesirable, as **6k–m** showed diminished affinity for ARTD3 and two compounds in the series showed selectivity toward ARTD1 or ARTD2 over ARTD3.

**2.3. Role of the Linker Region.** Focus was now shifted from the amide part of the compounds to the ethylene linker that connects the quinazolinone to the amide. By extending this


dx.doi.org/10.1021/jm401394u | J. Med. Chem. 2013, 56, 9556–9568

**Scheme 3. Synthesis of Intermediate 13**

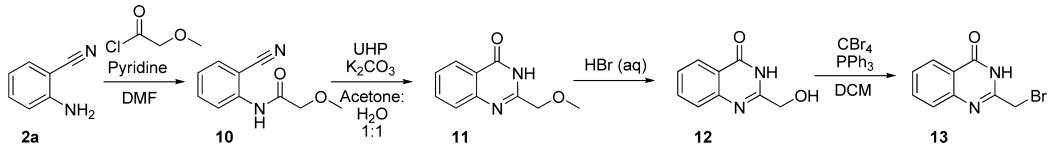


**Scheme 4. Synthesis of 7h,i**

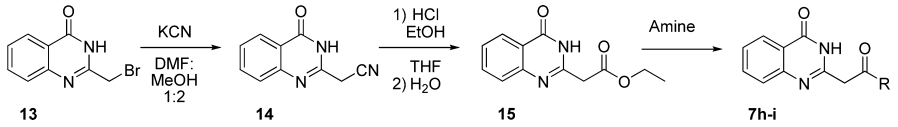


**Scheme 5. Synthesis of 7j,k**

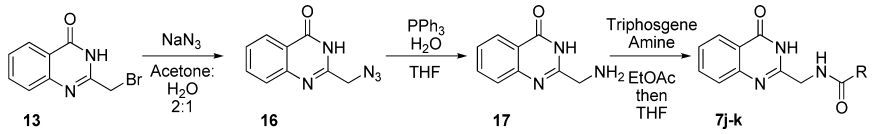


linker by one methylene group, it appeared possible to find interactions similar to those of **6j**. Synthesis of the required scaffold was straightforward by replacing succinic anhydride (Scheme 1) with glutaric anhydride and letting it react with 2-aminobenzonitrile, **2a**, to give **3c** in 84% yield. Compound **3c** was then ring-closed by the established procedure to give **4c** in 70% yield.

Forcing the ligand into a different binding pose by introducing a double bond (**7g**, Table 4) was expected to impair its affinity. In order to confirm this hypothesis, the compound was synthesized by letting 2-aminobenzonitrile **2a** react with fumaryl chloride in 66% yield. The resulting product, **8**, was then ring-closed in 36% yield to give **9** under the same conditions as in the previous cases (Scheme 2). The HATU-mediated amide couplings then proceeded in 9−81% yield to generate the first seven compounds. The low yields for some of the compounds were again attributed to difficulties with purification, as quantitative conversion of the carboxylic acid was generally observed.

Finally, the effects of a shorter linker (**7h,i**) and of additional possibilities for hydrogen bond formation by replacing the amide with a urea moiety (**7j,k**) were investigated. These four compounds shared the same synthetic pathway up to intermediate **13** (Scheme 3), after which the synthesis diverged in two separate directions. The synthesis of intermediate **13** started with the previously developed procedure, in which **2a** reacted with methoxyacetyl chloride to give **10** in 83% yield. Compound **10** was then ring-closed by use of UHP and potassium carbonate to give **11** in 77% yield. Subsequent ether cleavage by 47% HBr proceeded in 90% yield to give **12**, which was finally reacted under Appel reaction conditions with carbon tetrabromide and triphenylphosphine to obtain **13** in 84% yield.[17]

In order to synthesize **7h,i**, intermediate **13** was treated with potassium cyanide to produce nitrile **14** in 54% yield. The ester **15** was then obtained by dissolving **14** in ethanol and adding acetyl chloride to form the corresponding imino ether, which upon addition of water was hydrolyzed to the desired ester in 88% yield. Compounds **7h,i** were then obtained in 76−81% yield by direct transamidation of **15** (Scheme 4). Several other, more direct, methods of synthesizing **7h,i** were also investigated. All of these were unsuccessful, mainly due to the instability of **13** or of the carboxylic acid analogue of **15**.[18,19]

The two urea derivatives **7j,k** were synthesized by treating intermediate **13** with sodium azide to produce the azide analogue, **16**, in 98% yield. The azide was then reduced under Staudinger conditions with triphenylphosphine and water to generate the corresponding amine, **17**, in 89% yield. In the final step, the amines were reacted with triphosgene in order to obtain the desired isocyanates, which then reacted with **17** to form the desired urea derivatives in 38−42% yield (Scheme 5).

The elongated linker region of compounds **7a−f** (Table 4) resulted in reduced affinity across the board. However, the reduction was modest for all of these compounds with the exception of the **5b**-analogous **7b**, which produced a considerable drop in affinity. The thermal shift data suggested almost completely abolished binding for **7g** (Table 4), which confirmed the hypothesis that introduction of a double bond would force the ligand into an unfavorable binding pose with an associated decrease in affinity. Similar results were observed for the two compounds **7h** and **7i**, where the linker length was reduced by one methylene group. Finally, introducing an alternative hydrogen-bond acceptor by replacing the amide with a urea moiety did not seem to generate any new beneficial interactions, as affinity dropped considerably for **7j** compared to its amide analogue **5b**.

**2.4. Fine Tuning of Substituents.** Modifying the linker, changing the meso-methyl substituent to a different functionality, or introducing a substituent in the C7 position of the quinazolinone all had a negative impact on the ability of ligands to stabilize ARTD3. However, the effect of adding substituents to the phenyl ring still had to be investigated.

The crystal structure of ARTD3 in complex with **5b** (Figure 1a) was used to investigate which substituents would be accommodated at different positions. The structure suggested that ortho substituents larger than fluorine were unsuitable due to steric clashes with the protein. Similarly, meta substituents larger than a chlorine were also unlikely to fit inside the binding pocket without a major change of the binding pose. The para position would likely be able to accommodate larger substituents. However, as the thermal shift data for the two library substances **18h** and **18i** suggested that large substituents in this position would


dx.doi.org/10.1021/jm401394u | J. Med. Chem. 2013, 56, 9556−9568

Table 5. Thermal Shift Data for 18a–f against Five Members of the ARTD Family[a]

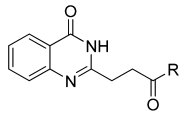

| Entry | ID | R | ARTD3 $\Delta T_m$ (°C) | ARTD1 $\Delta T_m$ (°C) | ARTD2 $\Delta T_m$ (°C) | ARTD5 $\Delta T_m$ (°C) | ARTD8 $\Delta T_m$ (°C) |
|---|---|---|---|---|---|---|---|
| 1 | **18a** | 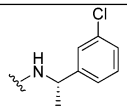 | 0.20 ± 0.08 | 0.26 ± 0.07 | -0.48 ± 0.14 | 0.29 ± 0.09 | -0.10 ± 0.19 |
| 2 | **18b** | 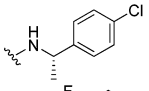 | 0.12 ± 0.07 | 0.04 ± 0.07 | -0.59 ± 0.05 | 0.18 ± 0.04 | 0.04 ± 0.20 |
| 3 | **18c** | 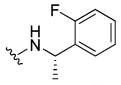 | 0.42 ± 0.24 | 0.36 ± 0.05 | -0.46 ± 0.64 | 0.12 ± 0.34 | 0.12 ± 0.16 |
| 4 | **18d** | 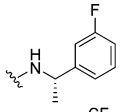 | 0.75 ± 0.14 | 1.00 ± 0.57 | 0.06 ± 0.56 | 0.13 ± 0.40 | -0.18 ± 0.14 |
| 5 | **18e** | 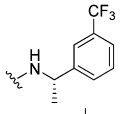 | 0.69 ± 0.27 | 0.25 ± 0.17 | -0.60 ± 0.16 | 0.23 ± 0.09 | -0.37 ± 0.10 |
| 6 | **18f** | 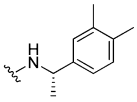 | 0.74 ± 0.13 | 0.22 ± 0.16 | -0.47 ± 0.19 | 0.22 ± 0.06 | -0.22 ± 0.20 |
| 7[a,b] | **18g** | 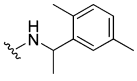 | 3.07 ± 0.19 | 2.00 ± 0.05 | 0.87 ± 0.17 | 0.44 ± 0.05 | 0.57 ± 0.09 |
| 8[a,b] | **18h** | 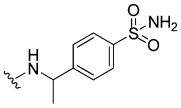 | 6.89 ± 0.35 | 3.36 ± 0.07 | 1.49 ± 0.19 | 1.94 ±0.06 | 0.02 ± 0.18 |
| 9[a,b] | **18i** | 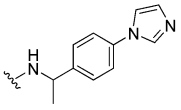 | 7.79 ± 0.19 | 6.17 ± 0.13 | 1.61 ± 0.43 | 0.64 ± 0.10 | 0.05 ± 0.14 |

[a]Commercial compounds. [b]Racemic mixture.

greatly increase the affinity for ARTD1, we decided not to introduce substituents larger than chlorine. Synthesis of **18a–f** (Table 5) was straightforward with yields of 50–97% for the final amide coupling step following the synthetic strategy that was already established for our previous ARTD3 ligands (Scheme 1).

Somewhat surprisingly, all compounds with small substituents on the phenyl ring (**18a–g**, Table 5) produced low thermal shifts, and binding to ARTD3 seemed almost completely abolished. This in combination with the low solubility observed during the preparation of the compounds suggest that they are less suited for further investigations.

**2.5. Exploring α-Amino Acid Analogues.** The fact that **6j**, based on phenylalaninol, proved to be a highly active compound while all other, considerably smaller modifications of **5b** decreased the affinity stirred our curiosity regarding the binding mode of this ligand. After the crystal structure of the complex was solved (Figure 2), it was clear that the amine part of **6j** had turned 180° compared to **5b** and **5d** (Figure 2), so that the phenyl ring was now pointing out of the binding pocket. In order to investigate whether this discovery could lead to further improvements over **5b**, a final series of compounds was synthesized by use of α-amino acid analogues as building blocks (Table 6). Synthesis of these compounds followed the previously established procedures with yields of 25–84% for the final amide coupling step (Scheme 1).

The first four members of this series of compounds (Table 6) showed reasonable thermal stabilization of the ARTDs (**19a–d**) but poor selectivity (**19b–d**). Compound **19e** seemed promising with similar thermal shifts as **5b**. However, in a cellular system the ester moiety would likely be converted to the corresponding carboxylic acid, **19f**, which showed poor ARTD3 affinity. The ester moiety in **19e** forces the compound to bind in a slightly shifted position in the nicotinamide pocket; however, the overall protein–ligand interaction seems tighter in the pocket (Figure S1 in Supporting Information). The two ester analogues, **19g** and **19h**, again showed modest affinity but, together with **19a**, seemed fairly selective toward ARTD3. The phenyl ring in **19a** has also turned around as in **6j**, and in addition, rigidifying the linker resulted in the phenyl ring reaching out even further out of the pocket, as observed in the crystal structure (Figure S1 in Supporting Information). Compound **19c** binds in a similar mode as **5b** but lacks the phenyl ring


dx.doi.org/10.1021/jm401394u | J. Med. Chem. 2013, 56, 9556–9568

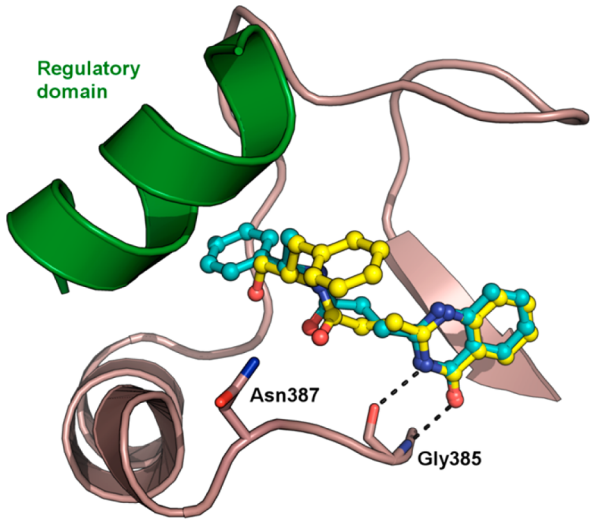


**Figure 2.** Compounds **6j** (yellow, PDB ID 4L7L) and **5b** (teal, PDB ID 4GV4) in ARTD3. The binding pose of the amine part is shifted compared to **5b**. The bifurcated interaction between the quinazolinone and the backbone of protein is still present, but the phenyl ring has turned around and is reaching out of the binding pocket. The interaction between Asn387 and the ligand also appears to be missing. The amide group has moved ~1 Å toward the position of the structured water in **5b**; this water is not present in the **6j** crystal structure.

structure, which might explain the smaller effect on $\Delta T_m$ observed for **19c** (Figure S1 in Supporting Information).

**2.6. Continued Characterization of Selected Compounds.** During the course of this medicinal chemistry project, the thermal shift assay was used exclusively for evaluating the presented compounds against a series of five ARTDs. To verify the results, an enzymatic assay was employed to further characterize and obtain half-maximal inhibitory concentration ($IC_{50}$) values for a subset of the most promising compounds (Table 7). The criterion for selecting these compounds was $\Delta T_m$ > 6.5 °C against ARTD3. Additional compounds for which we had obtained crystal complex structures were also analyzed in order to verify our conclusions about the importance of the stereochemistry and of the methyl group.

In brief, $Ni^{2+}$ chelating plates were used to capture hexahistidine-tagged ARTD catalytic domain fragments and recombinant histone proteins. Biotinylated $NAD^+$ was then added in order to initiate ADP-ribosylation. Reaction products were detected by chemiluminescence, and the assay was run with [$NAD^+$] near $K_m$ and in the presence of ARTD inhibitor. $IC_{50}$ determinations were conducted with ligand concentrations between 10 nM and 450 $\mu$M.

As expected, the analysis showed that $\Delta T_m$ values provide only a rough estimate of the potency and selectivity of a compound. While a moderately strong correlation between these two sets of results was observed for ARTD3, it was difficult to draw any such conclusions for ARTD1. $\Delta T_m$ values were also generally lower for ARTD1 compared to ARTD3 when similar $IC_{50}$ values were considered. However, our previous conclusions about how the stereochemistry of **5a–f** relates to the

**Table 6. Thermal Shift Data for 19a–h against Five Members of the ARTD Family**

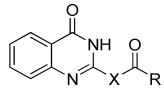

| Entry | ID | X | R | ARTD3 $\Delta T_m$ (°C) | ARTD1 $\Delta T_m$ (°C) | ARTD2 $\Delta T_m$ (°C) | ARTD5 $\Delta T_m$ (°C) | ARTD8 $\Delta T_m$ (°C) |
|---|---|---|---|---|---|---|---|---|
| 1 | **6j** | $CH_2CH_2$ | 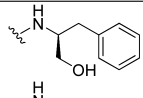 | 9.82 ± 0.39 | 3.59 ± 0.02 | 1.37 ± 0.17 | 0.60 ± 0.05 | 0.08 ± 0.16 |
| 2 | **19a** | (E)-CHCH | 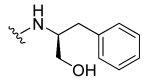 | 6.25 ± 0.07 | 0.41 ± 0.31 | -0.17 ± 0.32 | 0.08 ± 0.33 | -0.70 ± 0.08 |
| 3 | **19b** | $CH_2CH_2$ | 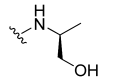 | 7.28 ± 0.19 | 3.43 ± 0.07 | 0.94 ± 0.19 | 0.56 ± 0.14 | 0.00 ± 0.14 |
| 4 | **19c** | $CH_2CH_2$ | 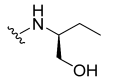 | 7.07 ± 0.30 | 2.88 ± 0.01 | 0.88 ± 0.34 | 0.35 ± 0.15 | 0.01 ± 0.07 |
| 5 | **19d** | $CH_2CH_2$ | 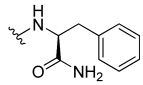 | 6.58 ± 0.17 | 3.09 ± 0.03 | 0.53 ± 0.16 | 1.08 ± 0.06 | 0.23 ± 0.04 |
| 6 | **19e** | $CH_2CH_2$ | 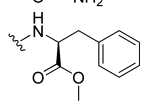 | 10.05 ± 0.70 | 1.75 ± 0.02 | 0.35 ± 0.25 | 0.50 ± 0.10 | -0.83 ± 0.20 |
| 7 | **19f** | $CH_2CH_2$ | 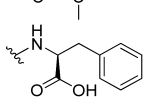 | 1.36 ± 0.10 | 0.24 ± 0.07 | -0.32 ± 0.10 | 0.22 ± 0.10 | -0.37 ± 0.08 |
| 8 | **19g** | $CH_2CH_2$ | 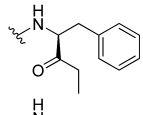 | 5.71 ± 0.47 | 1.93 ± 0.23 | 0.98 ± 0.14 | 0.07 ± 0.11 | 0.13 ± 0.21 |
| 9 | **19h** | $CH_2CH_2$ | 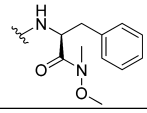 | 5.94 ± 0.57 | 1.37 ± 0.36 | 0.33 ± 0.09 | 0.11 ± 0.11 | 0.32 ± 0.11 |


dx.doi.org/10.1021/jm401394u | J. Med. Chem. 2013, 56, 9556–9568

Table 7. Effects of Selected Compounds on Catalytic Activities of ARTD3 and ARTD1[a]

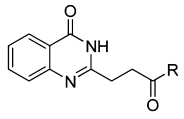

| Entry | ID | R | ARTD3 $\Delta T_m$ (°C) | ARTD1 $\Delta T_m$ (°C) | ARTD3 $IC_{50}$ (μM) | ARTD1 $IC_{50}$ (μM) |
|---|---|---|---|---|---|---|
| 1[a] | **5a** | 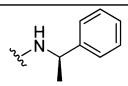 | 5.97 ± 0.47 | 3.05 ± 0.03 | 15.2 ± 10.0 | 0.51 ± 0.16<br>1.0 ± 0.10[b] |
| 2[a] | **5b** | 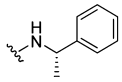 | 8.45 ± 0.59 | 1.80 ± 0.05 | 0.9 ± 0.3 | 3.70 ± 3.00<br>6.3 ± 0.62[b] |
| 3[a] | **5c** | 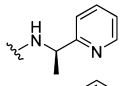 | 4.79 ± 0.21 | 2.35 ± 0.08 | >100[c] | 0.88 ± 0.34<br>0.9 ± 0.10[b] |
| 4[a] | **5d** | 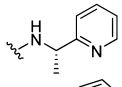 | 9.71 ± 0.39 | 1.96 ± 0.24 | 1.3 ± 0.2 | 2.12 ± 0.46<br>9.1 ± 2.6[b] |
| 5 | **5e** | 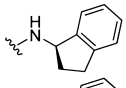 | 6.84 ± 0.14 | 2.37 ± 0.01 | >100[c] | 0.78 ± 0.26 |
| 6 | **5f** | 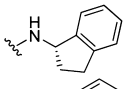 | 6.72 ± 0.49 | 2.38 ± 0.05 | >100[c] | 0.51 ± 0.11 |
| 7 | **6a** | 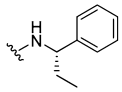 | 2.80 ± 0.15 | 1.49 ± 0.02 | 2.2 ± 0.6 | 0.14 ± 0.02 |
| 8 | **6j** | 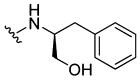 | 9.82 ± 0.39 | 3.59 ± 0.02 | 1 ± 0.3 | 6.46 ± 2.30 |
| 9 | **18h** | 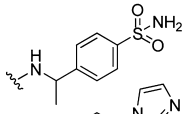 | 6.89 ± 0.35 | 3.36 ± 0.07 | 14.4 ± 4.00 | 1.50 ± 0.50 |
| 10 | **18i** | 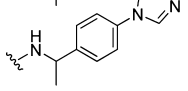 | 7.79 ± 0.19 | 6.17 ± 0.13 | 13.2 ± 6.00 | 0.45 ± 0.13 |
| 11 | **19b** |  | 7.28 ± 0.19 | 3.43 ± 0.07 | 11.1 ± 2.7 | 1.98 ± 1.40 |
| 12 | **19c** | 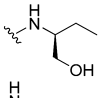 | 7.07 ± 0.30 | 2.88 ± 0.01 | 9.6 ± 1.0 | 3.10 ± 0.10 |
| 13 | **19d** | 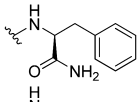 | 6.58 ± 0.17 | 3.09 ± 0.03 | 3.8 ± 1.4 | 0.70 ± 0.34 |
| 14 | **19e** | 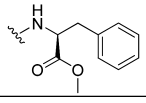 | 10.05 ± 0.70 | 1.75 ± 0.02 | 2.2 ± 0.3 | 2.50 ± 1.60 |

[a]Data were previously published for **5a** (ME0327), **5b** (ME0328), **5c** (ME0354), and **5d** (ME0355).[12] Full-length ARTD3 was used in all cases. ARTD1 catalytic domain fragment was used for all compounds, and the $IC_{50}$ determinations for **5a**–**d** were also expanded with full-length ARTD1.[12] [b]Full-length ARTD1. [c]We were unable to fit a curve to the data, but an $IC_{50}$ >100 μM is estimated.

ARTD1/ARTD3 selectivity were further reinforced by the $IC_{50}$ values: ARTD3 prefers the *S* enantiomer while ARTD1 prefers the *R* enantiomer. Out of the five α-amino acid analogues that were characterized, only **6j** showed any selectivity for ARTD3; the remaining four, **19b**–**e**, were unselective or ARTD1-selective despite what their $\Delta T_m$ values suggested.

Several crystal structures of ARTDs in complex with selected compounds were used throughout the study to guide selection of compounds, together with thermal shifts and $IC_{50}$ values, for further development. Compound **6a** has an ethyl group in place of the methyl on **5b**. The larger substituent did not change the mode of binding of **6a** (Figure S1 in Supporting Information). Placement of the library compounds **18h** and **18i** in the structures were also almost identical to **5b**, with the larger substituents on para position of the phenyl ring reaching into the pocket. One difference in the protein was seen; the side chain of Met402 shifted to accommodate the larger substituents.

## 3. CONCLUDING REMARKS

The potency and ARTD3 selectivity of the parent compound, **1**, was improved by systematically investigating how these two properties were affected by modifying different structural


dx.doi.org/10.1021/jm401394u | J. Med. Chem. 2013, 56, 9556–9568

features. The stereochemistry and the methyl group proved essential since the *S* enantiomer (**5d**) is ARTD3-selective while the *R* enantiomer (**5c**) is ARTD1-selective. Removal of the methyl group caused the thermal shifts to decrease, as exemplified by **5h**, and ring-closing to the indane produced ARTD1 selectivity for both enantiomers, as exemplified by **5e,f** (Table 2). Replacing this group with larger substituents also decreased the ARTD3 thermal shifts (Table 3). However, the pyridinyl moiety could be replaced by a phenyl group with an associated improvement of thermal shifts and selectivity (Table 2, compound **5d**). The linker region connecting this part to the quinazolinone scaffold was also investigated; however, none of these modifications improved binding properties (Table 4). Adding substituents to the phenyl ring also reduced the thermal shifts associated with these analogues (Table 5). Finally, a series based on $\alpha$-amino acid analogues as building blocks was synthesized and tested (Table 6), and a crystal structure showed that these compounds adopted a different binding pose (Figure 2). However, most of them showed poor selectivity, the exception being **6j**, which had binding properties comparable to those of **5d**.

A thermal shift assay was used throughout for compound profiling. However, in order to verify our conclusions, a subset of the best ARTD3 ligands was characterized with $IC_{50}$ values determined by an enzymatic activity assay. Using these assays, we successfully identified two compounds, **5b** ($IC_{50}$ = 0.9 $\mu$M against ARTD3 and 3.70 $\mu$M against ARTD1) and **6j** ($IC_{50}$ = 1.0 $\mu$M against ARTD3 and 6.46 $\mu$M against ARTD1), as potent and selective inhibitors of ARTD3. These compounds also maintain the advantageous low molecular weight and permeability of the parent compound, **1**. The $IC_{50}$ data also verified the intriguing relationship between stereochemistry and selectivity, where **5b** and **5d** are ARTD3-selective while their enantiomers **5a** and **5c** are ARTD1-selective. Finally, one of these compounds, **5b**, was characterized in cellular assays, proving that it is a potent and selective inhibitor of ARTD3 in vivo. No ARTD1 inhibitory effects were observed despite the modest selectivity suggested by the $IC_{50}$ values.[12]

While this compound shares structural features with several previously reported ARTD inhibitors, it is important to note that most of these previous compounds have been selective for ARTD1, -2, -5, or -6 and mostly lack chiral centers, which according to our study are important in order to differentiate between different ARTDs.[20−27]

## 4. EXPERIMENTAL SECTION

**4.1. General Chemical Procedures.** LC-MS analysis was carried out on a Waters LC system equipped with an Xterra MS C18 18.5 $\mu$m 4.6 × 50 mm column and an eluent system consisting of MeCN in water, both of which contained 0.2% formic acid. Detection was performed at 214 and 254 nm. Mass spectra were obtained by use of a Waters micromass ZG 2000, using both positive and negative electrospray ionization. $^1$H NMR and $^{13}$C NMR spectra were recorded on a Bruker DRX-400 spectrometer in $CDCl_3$ solution [residual $CHCl_3$ ($\delta_H$ 7.26 ppm, $\delta_C$ 77.16 ppm) as internal standard] or in $(CD_3)_2SO$ solution [residual $(CH_3)_2SO$ ($\delta_H$ 2.50 ppm, $\delta_C$ 39.52 ppm) as internal standard]. Optical rotations were measured on a Perkin-Elmer polarimeter 343 at 20 °C. A Biotage Initiator 400W was used for microwave heating. All target compounds were ≥95% pure according to LC-MS UV traces. Chiral HPLC was performed on a Beckman system equipped with a Pirkle Covalent (S,S) Whelk-O 1 10/100 Krom FEC 25 cm × 4.6 mm column or a Supelco Astec Chirobiotic T 25 cm × 4.6 mm, 7 $\mu$m column and an eluent system consisting of 2-propanol and hexane in a 1:1 ratio. Detection was performed at 254 nm with a System Gold 166 detector. Compounds **3a**, **4a**, **5a−d**, , **20a,b**, **21a**, and **21b** were synthesized according to procedures described in ref 14; analytical data were in agreement with those already published. Compound **10−12** were synthesized according to procedures described in ref 16; analytical data were in agreement with those already published.

**4.2. Synthetic Procedures.** *4.2.1. Procedure A: Acylation of Aniline (Exemplified by **3c**).* 2-Aminobenzonitrile (**2a**) (1500 mg, 12.7 mmol), and glutaric anhydride (1739 mg, 15.2 mmol) were dissolved in toluene (15 mL). The mixture was heated to 90 °C for 4 h under nitrogen. The solid material was filtered off and washed with $Et_2O$ to give **3b** (2476 mg, 84%). $^1$H NMR [400 MHz, $(CD_3)_2SO$] $\delta$ 12.08 (s, 1H), 10.14 (s, 1H), 7.80 (dd, $J$ = 7.8, 1.5 Hz, 1H), 7.68 (ddd, $J$ = 8.6, 7.3, 1.4 Hz, 1H), 7.54 (d, $J$ = 8.1 Hz, 1H), 7.34 (ddd, $J$ = 8.2, 6.6, 1.6 Hz, 1H), 2.41 (t, $J$ = 7.5 Hz, 2H), 2.31 (t, $J$ = 7.5 Hz, 2H), (quin, $J$ = 7.5 Hz, 2H); $^{13}$C NMR [100 MHz, $(CD_3)_2SO$] $\delta$ 174.1, 171.2, 140.2, 133.7, 133.1, 125.6, 125.6, 116.9, 107.6, 34.7, 32.8, 20.4.

*4.2.2. Procedure B: Cyclization of 2-Cyanoanilide (Exemplified by **4c**).* Compound **3c** (2316 mg, 9.97 mmol), $K_2CO_3$ (2756 mg, 19.94 mmol), and UHP (2815 mg, 29.94 mmol) were dissolved in acetone/$H_2O$ 1:1 (100 mL). The mixture was heated to 80 °C for 22 h. $K_2CO_3$ (2756 mg, 19.94 mmol) and UHP (2815 mg, 29.94 mmol) were added and the mixture was heated to 80 °C overnight. pH was adjusted to ∼4 with 6 M HCl. The solid material was filtered off and washed with MeOH and DCM to give **4c** (1626 mg, 70%). $^1$H NMR [400 MHz, $(CD_3)_2SO$] $\delta$ 12.16 (s, 1H), 12.09 (s, 1H), 8.07 (dd, $J$ = 7.9, 1.6 Hz, 1H), 7.76 (ddd, $J$ = 8.2, 7.2, 1.6 Hz, 1H), 7.60 (d, $J$ = 8.1 Hz, 1H), 7.45 (t, $J$ = 7.5 Hz, 1H), 2.64 (t, $J$ = 7.5 Hz, 2H), 2.32 (t, $J$ = 7.4 Hz, 2H), 1.96 (quin, $J$ = 7.5 Hz, 2H); $^{13}$C NMR [100 MHz, $(CD_3)_2SO$] $\delta$ 174.0, 161.7, 156.8, 148.8, 134.2, 126.8, 127.0, 125.7, 120.9, 33.5, 32.8, 21.8.

*4.2.3. Procedure C: Amide Coupling of $\alpha$-Methylbenzylamine (Exemplified by **18b**).* Compound **4a** (40 mg, 0.183 mmol), (*S*)-4-chloro-$\alpha$-methylbenzylamine (34.2 mg, 0.22 mmol), HATU (83.6 mg, 0.22 mmol), and TEA (61 $\mu$L, 0.44 mmol) were dissolved in DMF (1 mL), and the mixture was stirred at room temperature overnight. The solid residue was filtered off to give (*S*)-*N*-[1-(4-chlorophenyl)-ethyl]-3-(4-oxo-3*H*-quinazolin-2-yl)propanamide, **18b** (63 mg, 97%). $^1$H NMR [400 MHz, $(CD_3)_2SO$] $\delta$ 12.12 (s, 1H), 8.44 (d, $J$ = 7.8 Hz, 1H), 8.07 (dt, $J$ = 7.9 Hz, 1H), 7.78 (t, $J$ = 7.7 Hz, 1H), 7.55 (d, $J$ = 8.1 Hz, 1H), 7.46 (t, $J$ = 7.7 Hz, 1H), 7.27 (q, $J$ = 8.7 Hz, 4H), 4.87 (quin, $J$ = 7.2 Hz, 1H), 2.91−2.77 (m, 2H), 2.75−2.58 (m, 2H), 1.31 (d, $J$ = 7.0 Hz, 3H); $^{13}$C NMR [100 MHz, $(CD_3)_2SO$] $\delta$ 170.2, 161.6, 156.7, 148.7, 143.9, 134.2, 130.9, 128.0 (2C), 127.7 (2C), 126.7, 125.9, 125.7, 120.9, 47.3, 31.3, 29.6, 22.3.

*4.2.4. Procedure D: Appel Reaction (Exemplified by **13**).* Triphenylphosphine (152 mg, 0.58 mmol) was added to a mixture of **12** and $CBr_4$ (193 mg, 0.58 mmol) in DCM (8 mL) at 0 °C. The reaction was stirred at 0 °C for 1 h, and then triphenylphosphine (152 mg, 0.58 mmol) and $CBr_4$ (193 mg, 0.58 mmol) were added. The mixture was stirred at 0 °C for 1 h and then at room temperature for 20 h. Purification by column chromatography on silica gel (DCM/MeOH 96:4) followed by careful trituration with DCM to remove $PPh_3O$ gave 2-(bromomethyl)quinazolin-4(3*H*)-one, **13** (196 mg, 84%). $^1$H NMR [400 MHz, $(CD_3)_2SO_3$] $\delta$ 12.55 (s, 1H), 8.11 (dd, $J$ = 7.9, 1.5 Hz, 1H), 7.82 (ddd, $J$ = 8.0, 7.2, 1.6 Hz, 1H), 7.66 (d, $J$ = 8.2 Hz, 1H), 7.53 (t, $J$ = 7.5 Hz, 1H), 4.40 (s, 2H); $^{13}$C NMR [100 MHz, $(CD_3)_2SO_3$] $\delta$ 161.5, 152.8, 148.3, 134.6, 127.2 (2C), 125.8, 121.1, 29.7.

*4.2.5. Procedure E: Transformation of Nitrile to Ester via the Corresponding Imino Ether (Exemplified by **15**).* Compound **14** (55 mg, 0.30 mmol) was dissolved in a mixture of THF (0.3 mL) and ethanol (2.2 mL). AcCl (1.4 mL, 19.30 mmol) was added dropwise at 0 °C. The reaction was stirred at room temperature for 6 h and then concentrated under reduced pressure before water (1 mL) was added. The mixture was stirred at room temperature for 30 min and then concentrated and purified by column chromatography on silica gel (DCM/MeOH 99:1) to give ethyl 2-(4-oxo-3*H*-quinazolin-2-yl)-acetate, **15** (61 mg, 88%). $^1$H NMR (400 MHz, $CDCl_3$) $\delta$ 11.02 (s, 1H), 8.28 (d, $J$ = 7.8 Hz, 1H), 7.82−7.69 (m, 2H), 7.51 (t, $J$ = 7.5 Hz, 1H), 4.27 (q, $J$ = 7.2 Hz, 2H), 3.90 (s, 2H), 1.31 (t, $J$ = 7.2 Hz, 3H);


dx.doi.org/10.1021/jm401394u | J. Med. Chem. 2013, 56, 9556−9568

**Table 8. Statistics for Data Collection, Data Processing, and Structure Refinement of ARTD3−Compound Complexes**

| | 5i | 6a | 6j | 18h | 18i | 19a | 19c | 19e |
|---|---|---|---|---|---|---|---|---|
| | | | | Data Collection | | | | |
| beamline | Diamond I04 | Diamond I04 | Diamond I04 | Diamond I04 | Diamond I04 | Bessy BL14.1 | Bessy BL14.1 | Bessy BL14.1 |
| wavelength (Å) | 0.9919 | 0.9795 | 0.9795 | 0.9795 | 0.9795 | 0.918 41 | 0.918 41 | 0.918 41 |
| space group | $P2_1$ | $P2_1$ | $P2_1$ | $P2_1$ | $P2_1$ | $P2_1$ | $P2_1$ | $P2_1$ |
| unit cell dimensions $a$, $b$, $c$ (Å) | 55.27, 56.80, 56.63 | 55.06, 57.01, 56.69 | 55.17, 56.77, 56.64 | 54.95, 56.82, 56.43 | 54.52, 56.92, 56.84 | 56.88, 56.54, 58.62 | 55.32, 56.46, 56.48 | 55.19, 56.75, 56.91 |
| angles $\alpha$, $\beta$, $\gamma$ (deg) | 90.0, 112.6, 90.0 | 90.0, 112.4, 90.0 | 90.0, 112.5, 90.0 | 90.0, 112.4, 90.0 | 90.0, 112.4, 90.0 | 90.0, 114.3, 90.0 | 90.0, 113.0, 90.0 | 90.0, 112.1, 90.0 |
| resolution (Å) | 30.0−2.00 (2.05−2.00) | 30.0−2.00 (2.05−2.00) | 30.0−2.10 (2.15−2.10) | 30.0−1.80 (1.85−1.80) | 30.0−2.00 (2.05−2.00) | 30.0−2.30 (2.36−2.30) | 20.0−2.20 (2.26−2.20) | 30.0−2.80 (2.87−2.80) |
| unique reflns | 22 044 (1622) | 22 105 (1634) | 18 469 (1088) | 29 917 (2168) | 21 888 (1601) | 17 357 (2763) | 16 357 (2553) | 10 114 (1576) |
| $R$-merge (%)[a] | 12.1 (47.8) | 13.2 (57.5) | 14.2 (62.5) | 10.4 (60.6) | 12.2 (47.5) | 7.6 (60.3) | 6.8 (38.9) | 15.0 (62.9) |
| completeness (%) | 99.7 (98.9) | 99.7 (99.8) | 96.9 (78.3) | 99.7 (98.7) | 99.7 (99.6) | 99.5 (99.7) | 99.2 (96.1) | 99.2 (99.4) |
| redundancy | 7.4 (7.3) | 7.4 (7.2) | 7.0 (4.7) | 7.4 (7.2) | 7.4 (7.5) | 5.7 (5.7) | 4.6 (4.1) | 4.0 (4.1) |
| $\langle I \rangle / \langle \sum I \rangle$ | 16.2 (3.6) | 15.6 (3.1) | 13.9 (2.7) | 17.7 (2.8) | 15.9 (3.7) | 19.6 (3.2) | 19.3 (5.3) | 9.5 (3.0) |
| | | | | Refinement | | | | |
| resolution (Å) | 28.4−2.00 (2.05−2.00) | 28.5−2.00 (2.05−2.00) | 28.4−2.10 (2.16−2.10) | 28.4−1.80 (1.85−1.80) | 28.5−2.00 (2.05−2.00) | 20.8−2.30 (2.46−2.30) | 27.1−2.20 (2.35−2.20) | 27.4 −2.80 (3.13−2.80) |
| $R$-all[b] (%) | 16.39 | 16.78 | 17.42 | 16.03 | 16.52 | 18.74 | 17.95 | 24.24 |
| $R$-free[b] (%) | 20.95 | 21.64 | 22.29 | 19.81 | 21.00 | 23.38 | 22.74 | 28.81 |
| rmsd bond length (Å) | 0.017 | 0.017 | 0.018 | 0.020 | 0.019 | 0.010 | 0.010 | 0.010 |
| rmsd bond angle (deg) | 1.5 | 1.6 | 1.6 | 1.7 | 1.7 | 1.1 | 1.0 | 1.2 |
| Ramachandran plot[c]most favored (%) | 98.9 | 99.1 | 98 | 98.9 | 98.0 | 98.6 | 98.6 | 97.4 |
| Ramachandran plot[c]allowed (%) | 100 | 100 | 100 | 100 | 100 | 100 | 100 | 100 |

[a] $R_{merge} = \sum|I - \langle I \rangle| / \sum I$, where $I$ is the intensity measurement for a given reflection and $\langle I \rangle$ is the average intensity for multiple measurements of this reflection. [b] $R = \sum||F_{obs}| - |F_{calc}|| / \sum|F_{obs}|$, where $R$-free is calculated for a randomly chosen 5−10% of reflections that were not used for structure refinement and $R$-all is calculated for all reflections. [c] The Ramachandran plot was calculated by use of the Molprobity server (http://molprobity.biochem.duke.edu/).



dx.doi.org/10.1021/jm401394u | J. Med. Chem. 2013, 56, 9556−9568

$^{13}$C NMR (100 MHz, $CDCl_3$) $\delta$ 168.5, 162.1, 149.7, 147.9, 135.2, 127.5, 126.9, 126.7, 121.1, 62.4, 40.2, 14.2.

*4.2.6. Procedure F: Transamidation by Use of α-Methylbenzylamine (Exemplified by **7h**).* Compound **15** (15 mg, 0.065 mmol) and (*R*)-(+)-1-phenylethylamine (0.5 mL, 3.91 mmol) were stirred at 45 °C under nitrogen overnight. The precipitate was filtered off, washed with EtOAc, and dried in vacuo to give (*R*)-2-(4-oxo-3*H*-quinazolin-2-yl)-*N*-(1-phenylethyl)acetamide, **7h** (16 mg, 81%). $^1$H NMR [400 MHz, $(CD_3)_2SO$] $\delta$ 12.12 (s, 1H), 8.64 (d, *J* = 7.9 Hz, 1H), 8.09 (dd, *J* = 7.9, 1.5 Hz, 1H), 7.79 (ddd, *J* = 8.2, 7.1, 1.6 Hz, 1H), 7.59 (d, *J* = 8.1 Hz, 1H), 7.48 (ddd, *J* = 8.0, 7.2, 0.9 Hz, 1H), 7.40−7.29 (m, 4H), 7.26−7.20 (m, 1H), 4.93 (quin, *J* = 7.2 Hz, 1H), 3.59 (s, 1H), 1.39 (d, *J* = 7.0 Hz, 3H); $^{13}$C NMR [100 MHz, $(CD_3)_2SO$] $\delta$ 165.9, 161.6, 152.6, 148.7, 144.3, 134.2, 128.2 (2C), 126.7 (2C), 126.1, 126.0 (2C), 125.7, 120.9, 48.2, 41.9, 22.5.

*4.2.7. Procedure G: $S_N2$ Reaction at Benzylic Position (Exemplified by **16**).* Compound **13** (730 mg, 3.05 mmol) and $NaN_3$ (238 mg, 3.66 mmol) in acetone/water 2:1 (40 mL) was divided into two 10−20 mL vials and heated to 70 °C for 20 min by microwave irradiation. The solution was diluted with DCM and washed with brine. The organic phase was dried ($Na_2SO_4$), filtered, concentrated, and purified by column chromatography on silica gel (DCM/MeOH 98:2) gave 2-(azidomethyl)quinazolin-4(3*H*)-one, **16** (600 mg, 97%). $^1$H NMR [400 MHz, $(CD_3)_2SO_3$] $\delta$ 12.39 (s, 1H), 8.11 (dd, *J* = 7.9, 1.5 Hz, 1H), 7.83 (ddd, *J* = 8.2, 7.2, 1.6 Hz, 1H), 7.67 (d, *J* = 8.2 Hz, 1H), 7.53 (ddd, *J* = 8.0, 7.1, 0.9 Hz, 1H), 4.38 (s, 2H); $^{13}$C NMR [100 MHz, $(CD_3)_2SO_3$] $\delta$ 161.4, 152.3, 148.2, 134.5, 127.1, 126.8, 125.8, 121.3, 50.9.

*4.2.8. Procedure H: Staudinger Reduction (Exemplified by **17**).* Compound **16** (400 mg, 1.98 mmol) and triphenylphosphine (623 mg, 2.37 mmol) were dissolved in THF (10 mL), and $H_2O$ (0.53 mL, 29.65 mmol) was added. The mixture was stirred at room temperature under nitrogen for 19 h and then concentrated and purified by column chromatography on silica gel (DCM/MeOH 9:1) to give 2-(aminomethyl)quinazolin-4(3*H*)-one, **17** (309 mg, 89%). $^1$H NMR [400 MHz, $(CD_3)_2SO_3$] $\delta$ 8.10 (dd, *J* = 7.9, 1.3 Hz, 1H), 7.78 (ddd, *J* = 8.2, 7.1, 1.5 Hz, 1H), 7.62 (d, *J* = 8.0 Hz, 1H), 7.47 (ddd, *J* = 8.4, 7.4, 0.9 Hz, 1H), 5.43 (s, 2H), 3.65 (s, 2H); $^{13}$C NMR [100 MHz, $(CD_3)_2SO_3$] $\delta$ 161.7, 158.5, 148.7, 134.3, 126.7, 126.0, 125.8, 121.1, 44.7.

*4.2.9. Procedure I: Urea Derivative Synthesis Using Triphosgene (Exemplified by **7j**).* (*S*)-(−)-1-Phenylethylamine (26 μL, 0.206 mmol) was dissolved in EtOAc (1 mL), and triphosgene (30.5 mg, 0.103 mmol) was added. The solution was heated to 80 °C for 4 h in a sealed vial. The solvent was evaporated and THF (1 mL) was added, followed by **17** (30 mg, 0.17 mmol). The mixture was stirred at room temperature for 3 h and then concentrated and purified by column chromatography on silica gel (DCM/MeOH 95:5) to give (*S*)-1-[(4-oxo-3*H*-quinazolin-2-yl)methyl]-3-(1-phenylethyl)urea, **7j** (21 mg, 38%). $^1$H NMR [400 MHz, $(CD_3)_2SO$] $\delta$ 12.13 (s, 1H), 8.09 (dd, *J* = 7.9, 1.6 Hz, 1H), 7.80 (ddd, *J* = 8.4, 6.7, 1.5 Hz, 1H), 7.61 (d, *J* = 8.2 Hz, 1H), 7.48 (ddd, *J* = 8.1, 7.1, 0.9 Hz, 1H), 7.34−7.26 (m, 4H), 7.23−7.16 (m, 1H), 6.89 (d, *J* = 8.1 Hz, 1H), 6.37 (t, *J* = 5.7 Hz, 1H), 4.76 (quin, *J* = 7.4 Hz, 1H), 4.18 (d, *J* = 5.7 Hz, 2H), 1.34 (d, *J* = 7.0 Hz, 3H); $^{13}$C NMR [100 MHz, $(CD_3)_2SO$] $\delta$ 161.4, 157.3, 155.3, 148.5, 145.6, 134.4, 128.2 (2C), 126.8, 126.4, 126.2, 125.8 (2C), 125.7, 121.2, 48.7, 42.2, 23.3.

**4.3. Thermal Shift Assay.** Thermal shift assays were carried out with ARTD catalytic domain fragments as described in detail before.[12] The results are expressed as $\Delta T_m$ in degrees Celsius, indicating the shift in protein melting temperature upon ligand binding. Values reported are means ± SD of 2−3 independent determinations, each with three or more replicates.

**4.4. Protein Crystallization.** Crystals of ARTD3 complexes with compounds **5i**, **6a**, **6j**, **18h**, **18i**, **19a**, **19c**, and **19e** were obtained by the sitting drop vapor diffusion method in 96-well plates (Corning), similarly as previously described.[14]

**4.5. Data Collection, Structure Solution, and Refinement.** Crystals were briefly transferred to a cryo solution consisting of 1.7−2.0 M DL-malic acid, 0.1 M bis-tris-propane, pH 7.0, 20−25% (w/v) glycerol, 0.2 M sodium chloride, and 1−2 mM compound, and then frozen in liquid nitrogen. Diffraction data were collected on the frozen crystals on synchrotron beamlines I04 at Diamond (Oxfordshire, U.K.) and on BL14.1 at Bessy (Berlin, Germany). All data were indexed and integrated by use of XDS software.[28] Manual model building was done with Coot[29] and refinement with Refmac5[30] or Buster.[31] The refinement progress was monitored by decreasing *R* and $R_{free}$ values. Statistics for data collection, processing, and refinement can be are given in Table 8.

**4.6. Enzymatic Activity Assay.** ADP-ribosyltransferase activity was measured as described in detail before.[14]

## ■ ASSOCIATED CONTENT

### Ⓢ Supporting Information

Additional text and 54 figures, showing binding of inhibitors **6a**, **18h**, **18i**, **19a**, **19c**, and **19e** to ARTD3 and copies of NMR spectra and detailed experimental procedures for compounds **3b,c**, **4b,c**, **5e,f**, **6a−m**, **7a−k**, **8**, **9**, **13−17**, **18a−f**, **19a−h**, **22**, and **23**. This material is available free of charge via the Internet at http://pubs.acs.org.

### Accession Codes

Coordinates and structure factors for the crystal structures have been deposited in the Protein Data Bank under Accession Codes 4L7L (**6j**), 4L6Z (**5i**), 4L7N (**18h**), 4L7O (**18i**), 4L70 (**6a**), 4L7U (**19e**), 4L7R (**19c**), and 4L7P (**19a**).

## ■ AUTHOR INFORMATION

### Corresponding Author

*Phone +46-90-7869328; fax +46-90-7867655; email mikael.elofsson@chem.umu.se.

### Notes

The authors declare no competing financial interest.

## ■ ACKNOWLEDGMENTS

We thank the beamline staff at the Helmholtz-Zentrum Berlin (HZB) at BESSY II (Berlin, Germany) and the Diamond Light Source (Didcot, U.K.) for excellent support, and Martin Moche (Protein Science Facility, Karolinska Institutet, Stockholm, Sweden) for assistance with synchrotron data collection. This work was financed by the Swedish Foundation for Strategic Research (RBc08-0014). H.S. thanks the Structural Genomics Consortium for additional support.

## ■ ABBREVIATIONS USED

Ac, acetate; ADP, adenosine diphosphate; ARTD, diphtheria toxin-like ADP-ribosyltransferases; DCM, dichloromethane; DIC, *N*,*N*′-diisopropylcarbodiimide; DMF, *N*,*N*′-dimethylformamide; DMSO, dimethyl sulfoxide; DNA, deoxyribonucleic acid; DPPA, diphenyl phosphoryl azide; $EC_{50}$, effective concentration 50%; Et, ethyl; HATU, *O*-(7-azabenzotriazol-1-yl)-*N*,*N*,*N*′,*N*′-tetramethyluronium hexafluorophosphate; HOAt, 1-hydroxybenzotriazole; LC-MS, liquid chromatography mass spectrometry; mART, mono-ADP-ribose transferase; Me, methyl; $NAD^+$, nicotinamide adenine dinucleotide; PARP, poly(ADP-ribose) polymerase; PBS, phosphate-buffered saline; Ph, phenyl; TCEP, tris(2-carboxyethyl)phosphine; TEA, triethylamine; THF, tetrahydrofuran; $T_m$, midpoint of transition; UHP, urea hydrogen peroxide

## ■ REFERENCES

(1) Hottiger, M. O.; Hassa, P. O.; Lüscher, B.; Schüler, H.; Koch-Nolte, F. Toward a unified nomenclature for mammalian ADP-ribosyltransferases. *Trends Biochem. Sci.* **2010**, *35*, 208−219.

(2) Karlberg, T.; Langelier, M. F.; Pascal, J. M.; Schüler, H. Structural biology of the writers, readers, and erasers in mono- and poly(ADP-ribose) mediated signaling. *Mol. Aspects Med.* **2013**, *3*410881108.
(3) Kim, M. Y.; Zhang, T.; Kraus, W. L. Poly(ADP-ribosyl)ation by PARP-1: 'PAR-laying' $NAD^+$ into a nuclear signal. *Genes Dev.* **2005**, *19*, 1951−1967.
(4) Gibson, B. A.; Kraus, W. L. New insights into the molecular and cellular functions of poly(ADP-ribose) and PARPs. *Nat. Rev. Mol. Cell. Biol.* **2012**, *13*, 411−424.
(5) Bürkle, A. Poly(ADP-ribose). The most elaborate metabolite of $NAD^+$. *FEBS J.* **2005**, *272*, 4576−4589.
(6) Schreiber, V.; Dantzer, F.; Ame, J. C.; de Murcia, G. Poly(ADP-ribose): novel functions for an old molecule. *Nat. Rev. Mol. Cell Biol.* **2006**, *7*, 517−528.
(7) Hassa, P. O.; Hottiger, M. O. The diverse biological roles of mammalian PARPs, a small but powerful family of poly-ADP-ribose polymerases. *Front. Biosci.* **2008**, *13*, 3046−3082.
(8) Underhill, C.; Toulmonde, M.; Bonnefoi, H. A review of PARP inhibitors: from bench to bedside. *Ann. Oncol.* **2011**, *22*, 268−279.
(9) Ekblad, T.; Camaioni, E.; Schüler, H.; Macchiarulo, A. PARP inhibitors: polypharmacology vs selective inhibition. *FEBS J.* **2012**, *280*, 3563−3575.
(10) Wahlberg, E.; Karlberg, T.; Kouznetsova, E.; Markova, N.; Macchiarulo, A.; Thorsell, A.; Pol, E.; Frostell, Å.; Ekblad, T.; Öncü, D.; Kull, B.; Robertson, G.; Pellicciari, R.; Schüler, H.; Weigelt, J. Family wide chemical profiling and structural analysis of PARP and Tankyrase inhibitors. *Nat. Biotechnol.* **2012**, *30*, 283−288.
(11) Lehtiö, L.; Jemth, A. S.; Collins, R.; Loseva, O.; Johansson, A.; Markova, N.; Hammarström, M.; Flores, A.; Holmberg-Schiavone, L.; Weigelt, J.; Helleday, T.; Schüler, H.; Karlberg, T. Structural basis for inhibitor specificity in human poly(ADP-ribose) polymerase-3. *J. Med. Chem.* **2009**, *52*, 3108−3111.
(12) Lindgren, A. E. G.; Karlberg, T.; Thorsell, A.-G.; Hesse, M.; Spjut, S.; Ekblad, T.; Andersson, C. D.; Pinto, A. F.; Weigelt, J.; Hottiger, M. O.; Linusson, A.; Elofsson, M.; Schüler, H. A PARP inhibitor with selectivity toward ADP-ribosyltransferase ARTD3/PARP3. *ACS Chem. Biol.* **2013**, *8*, 1698−1703.
(13) Several of the major retailers of fine chemicals were investigated.
(14) Bavetsias, V. A facile route to quinazolin-4(3*H*)-ones functionalised at the 2-position. *Synth. Commun.* **1998**, *28*, 4547−4559.
(15) Valeur, E.; Bradley, M. Amide bond formation: beyond the myth of coupling reagents. *Chem. Soc. Rev.* **2009**, *38*, 606−631.
(16) Staudinger, H.; Meyer, J. Über neue organische Phosphorverbindungen III. Phosphinmethylenderivate und Phosphinimine. *Helv. Chim. Acta* **1919**, *2*, 635−646.
(17) Appel, R. Tertiary phosphane/tetrachloromethane, a versatile reagent for chlorination, dehydration, and P-N linkage. *Angew. Chem., Int. Ed.* **1975**, *14*, 801−811.
(18) Xu, W.; Fu, H. Amino acids as the nitrogen-containing motifs in copper-catalyzed domino synthesis of N-heterocycles. *J. Org. Chem.* **2011**, *76*, 3846−3852.
(19) Other methods that were attempted: reaction of **2a** with ethyl(chloroformyl) acetate followed by cyclization to give **15** in two steps; palladium-catalyzed aminocarbonylation of **13**; acidic hydrolysis of **14** to the corresponding carboxylic acid; and CuBr-catalyzed synthesis of the carboxylic acid analogue of **15** starting from 2-bromobenzamide and L-aspartic acid. All of these worked poorly or not at all.
(20) Bregman, H.; Gunaydin, H.; Gu, Y.; Schneider, S.; Wilson, C.; DiMauro, E. F.; Huang, X. Discovery of a class of novel tankyrase inhibitors that bind to both the nicotinamide pocket and the induced pocket. *J. Med. Chem.* **2013**, *56*, 1341−1345.
(21) Hattori, K.; Kido, Y.; Yamamoto, H.; Ishida, J.; Iwashita, A.; Mihara, K. Rational design of conformationally restricted quinazolinone inhibitors of poly(ADP-ribose)polymerase. *Bioorg. Med. Chem. Lett.* **2007**, *17*, 5577−5581.
(22) Ishida, J.; Yamamoto, H.; Kido, Y.; Kamijo, K.; Murano, K.; Miyake, H.; Ohkubo, M.; Kinoshita, T.; Warizaya, M.; Iwashita, A.; Mihara, K.; Matsuoka, N.; Hattori, K. Discovery of potent and selective PARP-1 and PARP-2 inhibitors: SBDD analysis via a combination of X-ray structural study and homology modeling. *Bioorg. Med. Chem.* **2006**, *14*, 1378−1390.
(23) Iwashita, A.; Hattori, K.; Yamamoto, H.; Ishida, J.; Kido, Y.; Kamijo, K.; Murano, K.; Miyake, H.; Kinoshita, T.; Warizaya, M.; Ohkubo, M.; Matsuoka, N.; Mutoh, S. Discovery of quinazolinone and quinoxaline derivatives as potent and selective poly(ADP-ribose) polymerase-1/2 inhibitors. *FEBS Lett.* **2005**, *579*, 1389−1393.
(24) Shulz, M. D.; Cheung, A. K.; Kirby, C. A.; Firestone, B.; Fan, J.; Chen, C. H.; Chen, Z.; Chin, D. N.; DiPietro, L.; Fazal, A.; Fend, Y.; Fortin, P. D.; Gould, T.; Lagu, B.; Lei, H.; Lenoir, F.; Majumdar, D.; Ochala, E.; Palermo, M. G.; Pham, L.; Pu, M.; Smith, T.; Stams, T.; Tomlinson, R. C.; Touré, B. B.; Visser, M.; Wang, R. M.; Waters, N. J.; Shao, W. Identification of NVP-TNKS656: The use of structure-efficiency relationships to generate a highly potent, selective, and orally active tankyrase inhibitor. *J. Med. Chem.* **2013**, *56*, 6495−6511.
(25) Pellicciari, R.; Camaioni, E.; Costantino, G.; Formentini, L.; Sabbatini, P.; Venturoni, F.; Eren, G.; Bellocchi, D.; Chiarugi, A.; Moroni, F. On the way to selective PARP-2 inhibitors. Design, synthesis, and preliminary evaluation of a series of isoquinolinone derivatives. *ChemMedChem* **2008**, *3*, 914−923.
(26) Perkins, E.; Sun, D.; Nguyen, A.; Tulac, S.; Francesco, M.; Tavana, H.; Nguyen, H.; Tugendreich, S.; Barthmaier, P.; Couto, J.; Yeh, E.; Thode, S.; Jarnagin, K.; Jain, A.; Morgans, D.; Melese, T. Novel inhibitors of poly(ADP-ribose) polymerase/PARP1 and PARP2 identified using a cell-based screen in yeast. *Cancer Res.* **2001**, *61*, 4175−4183.
(27) Hattori, K.; Ishida, J.; Iwashita, A.; Kamijo, K.; Kido, Y.; Matsuoka, N.; Miyake, H.; Nakanishi, I.; Ohkuno, M.; Yamamoto, H.; Yamazaki, S. Quinazolinone derivatives. Patent Application PCT/JP2001/010601, 2002.
(28) Kabsch, W. XDS. *Acta Crystallogr., Sect. D: Biol. Crystallogr.* **2010**, *66*, 125−132.
(29) Emsley, P.; Lohkamp, B.; Scott, W. G.; Cowtan, K. Features and development of Coot. *Acta Crystallogr., Sect. D: Biol. Crystallogr.* **2010**, *66*, 486−501.
(30) Murshudov, G. N.; Skubák, P.; Lebedev, A. A.; Pannu, N. S.; Steiner, R. A.; Nicholls, R. A.; Winn, M. D.; Long, F.; Vagin, A. A. REFMAC5 for the refinement of macromolecular crystal structures. *Acta Crystallogr., Sect. D: Biol. Crystallogr.* **2011**, *67*, 355−367.
(31) Bricogne, G.; Blanc, E.; Brandl, M.; Flensburg, C.; Keller, P.; Paciorek, W.; Roversi, P.; Sharff, A.; Smart, O. S.; Vonrhein, C.; Womack, T. O. *BUSTER, version 2.11.5*; Global Phasing Ltd., Cambridge, U.K., 2011.